Parameter estimation of correlated photon pairs

Internship report

submitted by

Jan Gößwein

Registration number 212968

Supervisors: Prof. Dr. Thomas Pertsch
Dr. Frank Setzpfandt
M.Sc.? Masoud Safari Arabi

Institute: Insitute of Applied Physics

Contents

Glossary

Abbreviation	Description	Page
BBO	beta-barium borate	2, 10
BPM	birefringent phase matching	2
CAR	Coincidence-to-Accidentals ratio	10, 11
KTP	potassium titanyl phosphate	2
LN	lithium niobate	2
mmBE	multi-mode Bose-Einstein	9, 13, 14
QPM	quasi phase matching	2
SPDC	Spontaneous parametric down-conversion	1–3, 5, 8–10

1. Introduction

In recent years, quantum technologies have influenced several fields, including communication, computing, sensing, and imaging. They all have one thing in common: they utilize the non-classical properties of particles to improve state-of-the-art technology beyond its existing limits.
Specifically, in quantum imaging and sensing, the quantum nature of light is exploited, so light is considered not only as electromagnetic waves, but also as single photons.
In classical imaging, constraints such as the diffraction limit and shot noise limit system parameters like spatial resolution, sensitivity, and required illumination intensity. Quantum imaging aims to address some of these constraints by making use of quantum correlations, such as entanglement, photon-number correlations, and squeezing [3, 15].
Among the available quantum light sources, Spontaneous parametric down-conversion (SPDC) is widely used to generate photon pairs that are correlated in various degrees of freedom, including time, space, and polarization [15].
One example of an imaging technique that uses spatially correlated photons is Quantum ghost imaging. In this technique, an image of an object is reconstructed by measuring the intensity correlations between two spatially separated light beams produced by SPDC. One beam interacts with the sample but is detected without spatial information. The other beam, which does not interact with the sample, is measured with a spatially resolving detector. The spatial information about the sample is recovered by considering the spatial correlation between the two photon beams [6, 13].
Another imaging technique uses temporally correlated photons. These photons are particularly important in detection schemes based on coincidence measurements. For example, in a transmission setup, temporally correlated photon pairs can be used to estimate the characteristic properties of a sample.
One photon of the pair is sent through the sample while the other is detected directly. Coincidence measurements between the two detection events identify photons that were truly part of a pair. This suppresses uncorrelated background noise [15].
It has been shown that this approach has advantages over the conventional method, in which only photons passing through the sample are detected, and correlations are not considered [references???]. For certain biological samples, such as living cells, it is necessary that the wavelength of photons is in the mid-infrared (MIR) to ensure a non-destructive interaction with the sample. This wavelength range corresponds to fundamental vibrational absorption bands [8, 9].
However, a major technical challenge in the MIR regime is that the detectors have a low sensitivity and the level of noise is significantly high. In particular, thermal background radiation lead to high dark count rates and low signal-to-noise ratios (SNRs) [SNSPD/SPD reference].
This work aims to determine if measurements using temporally correlated photon pairs still

offer advantages over conventional single-photon experiments in regimes of large noise. First, the mechanism behind producing correlated photon pairs is explained. Then, a procedure for modeling the precision of the transmission parameter is introduced for both the correlation-based and conventional approaches. Next, the statistics of the necessary parameters are explained, as well as the setup used to verify those statistics experimentally. Furthermore, the experimental results are compared with the theoretical predictions. Finally, different parameter regions are simulated in order to find combinations for which the correlation-based approach is superior using the experimental results.

2. Theory

2.1. Spontaneous parametric down-conversion

To exploit the advantages of quantum imaging and sensing, one needs to create correlated biphoton states of light. The most efficient technology to create such quantum states are sources using Spontaneous parametric down-conversion (SPDC). The underlying process is as follows: an incident pump photon with frequency ω_p causes a nonlinear material response resulting in the spontaneous emission of a photon pair with lower frequencies ω_s and ω_i. The subscripts i and s represent the signal and idler photons, as they are usually referred to.
Most experiments use crystals, such as potassium titanyl phosphate (KTP) and beta-barium borate (BBO), or lithium niobate (LN) based optical waveguides, because they exhibit second-order nonlinearity [4, 12, 17]. To achieve efficient SPDC processes, the energy and momentum must be conserved. This means that the photon pair must interfere constructively and fulfill the phase-matching conditions of the wave vector $\vec{k}$ [6] :

$$\begin{aligned} \omega_\mathrm{p} &= \omega_\mathrm{s} + \omega_\mathrm{i} \\ \vec{k}_\mathrm{p} &= \vec{k}_\mathrm{s} + \vec{k}_\mathrm{i} - \Delta\vec{k} \end{aligned} \tag{2.1}$$

where the indices p, s and i refer to the pump, signal and idler photon. Δk represents the phase mismatch caused by dispersion, which results in zero produced photon pairs. There are two approaches to compensate for the mismatch.
One is called quasi phase matching (QPM) and exploits that in periodically poled crystals, e.g. KTP or LN, the nonlinear response also changes periodically, resulting in a phase mismatch of $\Delta k = 0$. It allows for a process called type-0 SPDC to happen, which means that all three photons (pump, signal, idler) have the same polarization direction.
Another way to compensate the mismatch is called birefringent phase matching (BPM) and uses anisotropic materials, such as BBO, as the refractive index changes with the polarization of the incident photon. The effect of using BPM is that the extraordinary photon is always polarized perpendicular to the pump. Therefore, no type-0 SPDC can be achieved

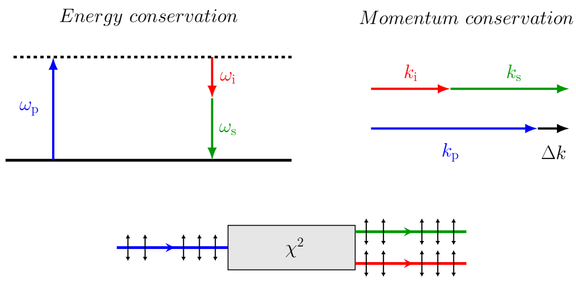

Figure 1.: Conservation processes of collinear Type-0 SPDC

with this approach. The two other possible cases are called type-I SPDC, which means that the signal and idler photons share the same polarization and are polarized perpendicular to the pump. Type-II SPDC means that the signal and idler photons are polarized perpendicular to each other [2]. A visualization of the conservation processes is shown in Figure 1.

In experiments, the temporal correlation between the signal and idler photons is most commonly used for coincidence measurements. These measurements are visualized as a histogram of photon detection events. These histograms plot the number of coincident detection events as a function of the delay between the arrival times of detections at two single-photon detectors.

Ideally, the temporal correlation of the photon pairs results in a distinct coincidence peak centered at zero delay if both detectors are the same distance from the SPDC source. The width of this peak depends on several factors, including the resolution of the time-tagging electronics that create a timestamp for each detection event.

These correlations are evaluated by defining a temporal interval around the detection peak. Within this interval, detection events are considered true coincidences, meaning they originate from the same photon pair. This interval is usually referred to as the coincidence window τ_{cw}. Events that fall outside this window are usually attributed to uncorrelated background noise and are called accidental counts. A representative scheme of a coincidence histogram is shown in Figure 2 .

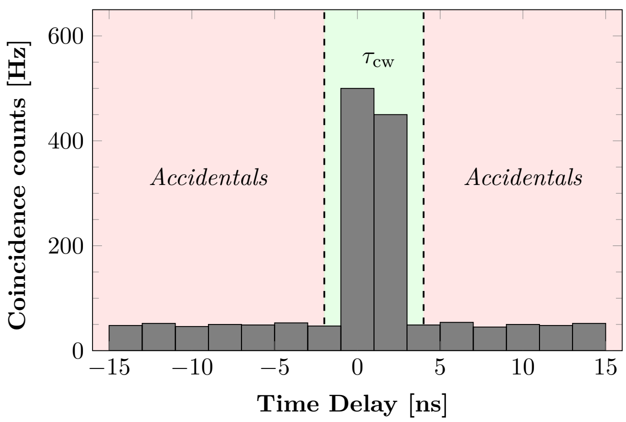

Figure 2.: Schematic of a coincidence histogram

2.2. Transmission variance model

When noise is present in the experimental setup, the question arises as to how precisely the parameters of interest can be determined using either the single or coincidence approach. As the objective of this work is to compare the precision of both methods rather than their absolute values, it is the variance of the chosen parameter that is decisive. As the results of this study will be used in a transmission setup, the chosen parameter is the transmission.
In the following, the formulas to calculate the variance of the transmission are derived both for the approach using singles and coincidences. The arm in which the sample is placed will be referred to as idler and the reference arm as signal. The case in which a sample is placed in the idler arm is denoted with the superscript 'sam', when no sample is placed with 'ref'.
Starting with the approach using singles, only the idler arm is required. Therefore, if no sample is placed, the number of total detected counts in this arm is:

$$N_{\text{tot}}^{\text{ref}} = \eta_{\text{idl}}\, N_g + N_{\text{noise}}^{\text{ref}} \tag{2.2}$$

where $N_{\text{tot}}^{\text{ref}}$ is the total number of counts without a sample, η_{idl} is the efficiency of the idler arm, N_g is the number of generated single photons and $N_{\text{noise}}^{\text{ref}}$ is the noise of the setup consisting of e.g. dark counts of the detector or stray light.
When a sample is placed in the idler arm the total number of counts changes according to the transmission characteristics of the material. Therefore, Equation 2.2 is modified as follows:

$$N_{\text{tot}}^{\text{sam}} = T\, \eta_{\text{idl}}\, N_g + N_{\text{noise}}^{\text{sam}} \tag{2.3}$$

where $N_{\text{tot}}^{\text{sam}}$ represents the total counts with a sample and T is the transmission of the sample.
The transmission T of the sample can be calculated combining equations 2.2 and 2.3:

$$T = \frac{N_{\text{tot}}^{\text{sam}} - N_{\text{noise}}^{\text{sam}}}{N_{\text{tot}}^{\text{ref}} - N_{\text{noise}}^{\text{ref}}} \tag{2.4}$$

As can be seen from the formula, four independent measurements must be conducted to retrieve the transmission: two where only the dark counts are measured with and without the sample, and two with an active laser also with and without the sample.

Based on Equation 2.4 and error propagation, the variance of the transmission $\mathrm{Var}(T)$ can be calculated assuming that all four variables are independent of each other [11]:

$$\begin{aligned}\mathrm{Var}(T) &= \sum_i \left(\frac{\partial T}{\partial X_i}\right)^2 \mathrm{Var}(X_i) \\ &= \left(\frac{\partial T}{\partial N_{\mathrm{tot}}^{\mathrm{sam}}}\right)^2 \mathrm{Var}(N_{\mathrm{tot}}^{\mathrm{sam}}) + \left(\frac{\partial T}{\partial N_{\mathrm{noise}}^{\mathrm{sam}}}\right)^2 \mathrm{Var}(N_{\mathrm{noise}}^{\mathrm{sam}}) \\ &\quad + \left(\frac{\partial T}{\partial N_{\mathrm{tot}}^{\mathrm{ref}}}\right)^2 \mathrm{Var}\left(N_{\mathrm{tot}}^{\mathrm{ref}}\right) + \left(\frac{\partial T}{\partial N_{\mathrm{noise}}^{\mathrm{ref}}}\right)^2 \mathrm{Var}\left(N_{\mathrm{noise}}^{\mathrm{ref}}\right)\end{aligned} \tag{2.5}$$

When the partial derivatives are explicitly calculated using Equation 2.4 the final formula for the variance of the tranmission is:

$$\begin{aligned}\mathrm{Var}(T) &= \frac{1}{(N_{\mathrm{tot}}^{\mathrm{ref}} - N_{\mathrm{noise}}^{\mathrm{ref}})^2}\left[\mathrm{Var}(N_{\mathrm{tot}}^{\mathrm{sam}}) + \mathrm{Var}(N_{\mathrm{noise}}^{\mathrm{sam}})\right] \\ &\quad + \frac{(N_{\mathrm{tot}}^{\mathrm{sam}} - N_{\mathrm{noise}}^{\mathrm{sam}})^2}{(N_{\mathrm{tot}}^{\mathrm{ref}} - N_{\mathrm{noise}}^{\mathrm{ref}})^4}\left[\mathrm{Var}\left(N_{\mathrm{tot}}^{\mathrm{ref}}\right) + \mathrm{Var}\left(N_{\mathrm{noise}}^{\mathrm{ref}}\right)\right]\end{aligned} \tag{2.6}$$

When using the coincidence approach, the formulas for the transmission and it's variance differ. Not only the idler arm, but also the signal arm is used to detect correlated photons created by SPDC. Assuming perfectly correlated photon pairs, the formula for pure coincidence counts with and without a sample in the idler arm is as follows [7]:

$$\begin{aligned}N_{\mathrm{cc}}^{\mathrm{pure,sam}} &= T\,\eta_{\mathrm{idl}}\,\eta_{\mathrm{sig}}\,N_g, \\ N_{\mathrm{cc}}^{\mathrm{pure,ref}} &= \eta_{\mathrm{idl}}\,\eta_{\mathrm{sig}}\,N_g\end{aligned} \tag{2.7}$$

where $\eta_{\mathrm{sig/idl}}$ is the efficiency of signal and idler arm, T is the transmission of the sample and N_g is the number of generated photon pairs.

In the context of coincidence measurements, it is important to note that the detection of pure coincidences is not the only outcome of such measurements. In addition to these, what is called accidental counts are also detected. Consequently, instead of both photons originating from one pair being detected simultaneously, only one is detected in one arm and a noise photon is detected in the other.Another possibility is that two photons are detected concurrently in both arms, yet neither of them originates from a SPDC-pair. In both cases, the time tagging unit recognizes them as coincidence events. Hence, they are designated as accidental counts.

The following formula is used to calculate accidental counts with sample ($N_{\text{ac}}^{\text{sam}}$) and without $\left(N_{\text{ac}}^{\text{ref}}\right)$ [7]:

$$\begin{aligned} N_{\text{ac}}^{\text{sam}} &= \left(T\,\eta_{\text{idl}} N_g + N_{\text{dc,idl}} - N_{\text{cc}}^{\text{pure,sam}}\right)\left(\eta_{\text{sig}} N_g + N_{\text{dc,sig}} - N_{\text{cc}}^{\text{pure,sam}}\right)\tau_{\text{cw}} \\ N_{\text{ac}}^{\text{ref}} &= \left(\eta_{\text{idl}} N_g + N_{\text{dc,idl}} - N_{\text{cc}}^{\text{pure,ref}}\right)\left(\eta_{\text{sig}} N_g + N_{\text{dc,sig}} - N_{\text{cc}}^{\text{pure,ref}}\right)\tau_{\text{cw}} \end{aligned} \tag{2.8}$$

Is that right with Ng or Rg??

where $N_{\text{dc,idl/sig}}$ denotes the dark counts in the idler/signal arm and τ_{cw} is the coincidence window, which represents the time range in which counts are considered to be pure coincidences.
Therefore, the measured total coincidence events are the sum of pure and accidental coincidence events:

$$\begin{aligned} N_{\text{tot,cc}}^{\text{sam}} &= N_{\text{cc}}^{\text{pure,sam}} + N_{\text{ac}}^{\text{sam}}, \\ N_{\text{tot,cc}}^{\text{ref}} &= N_{\text{cc}}^{\text{pure,ref}} + N_{\text{ac}}^{\text{ref}} \end{aligned} \tag{2.9}$$

Using equations 2.7, 2.8 and 2.9, the transmission T in the coincidence approach can be obtained as follows:

$$T = \frac{N_{\text{tot,cc}}^{\text{sam}} - N_{\text{ac}}^{\text{sam}}}{N_{\text{tot,cc}}^{\text{ref}} - N_{\text{ac}}^{\text{ref}}} \tag{2.10}$$

In comparison with the approach that utilizes single counts from Equation 2.4, which necessitates four independent measurements, this approach requires only two: one with and one without the sample. This is due to the fact that accidentals and coincidences can be obtained within a single measurement.
Since the objective is to compare the precision of the transmission T using the two different approaches, analogue to Equation 2.5, the variance of the transmission can be calculated using error propagation and coincidence counts:

$$\begin{aligned} \text{Var}(T) &= \sum_i \left(\frac{\partial T}{\partial X_i}\right)^2 \text{Var}(X_i) \\ &= \left(\frac{\partial T}{\partial N_{\text{tot,cc}}^{\text{sam}}}\right)^2 \text{Var}\left(N_{\text{tot,cc}}^{\text{sam}}\right) + \left(\frac{\partial T}{\partial N_{\text{ac}}^{\text{sam}}}\right)^2 \text{Var}(N_{\text{ac}}^{\text{sam}}) \\ &\quad + \left(\frac{\partial T}{\partial N_{\text{tot,cc}}^{\text{ref}}}\right)^2 \text{Var}\left(N_{\text{tot,cc}}^{\text{ref}}\right) + \left(\frac{\partial T}{\partial N_{\text{ac}}^{\text{ref}}}\right)^2 \text{Var}\left(N_{\text{ac}}^{\text{ref}}\right) \end{aligned} \tag{2.11}$$

Using equations 2.7 and 2.9, an explicit expression for the variance of the transmission can be obtained:

$$\mathrm{Var}(T) = \left(\frac{1}{\eta_{\mathrm{sig}}\,\eta_{\mathrm{idl}}\,N_g}\right)^2 \left[\mathrm{Var}\Big(N^{\mathrm{sam}}_{\mathrm{tot,cc}}\Big) + \mathrm{Var}(N^{\mathrm{sam}}_{\mathrm{ac}}) + T^2\Big(\,\mathrm{Var}\Big(N^{\mathrm{ref}}_{\mathrm{tot,cc}}\Big) + \mathrm{Var}\Big(N^{\mathrm{ref}}_{\mathrm{ac}}\Big)\,\Big)\right] \tag{2.12}$$

The objective of this work is to ascertain parameter configurations in which the coincidence approach exhibits superiority in terms of precision, as measured by the magnitude of the variance of the transmission, in comparison to the single approach. In order to model both variance formulas properly, it is necessary to experimentally investigate the statistics of each parameter of which the variance is calculated.

2.3. Statistics of photon counts

When investigating the statistical properties of photons, it is essential to recognize that different types of light sources exhibit distinct statistical distributions. These distributions are typically characterized by their respective variances, which serve as key indicators of the underlying photon statistics. A coherent laser source is often used as the reference standard, as it represents the most stable form of light emission within the picture of classical optics [5]. In the following, two types of light sources with fundamentally different statistical distributions are examined in greater detail, namely coherent and thermal sources.

2.3.1. Coherent light

From a classical perspective, a coherent light field, such as that produced by a stable laser, may be regarded as a monochromatic electromagnetic wave with well-defined amplitude and phase.

When considering a light beam of constant power P, the photon flux is uniform in time. To describe the detection statistics, the observation time interval T may be subdivided into a large number of subintervals of duration Δt. For each subinterval, the probability of detecting a single photon is small but finite. The probability of detecting two or more photons within a single subinterval can be neglected.

Since the intensity of the beam is constant, the detection probability is identical for each subinterval, and successive detection events are statistically independent.

The probability of detecting n photons within N subintervals of the total observation time T corresponds to the case where n subintervals each contain exactly one photon, while the remaining $(N-n)$ subintervals contain none. This situation is described by the binomial distribution [5]:

$$\mathcal{P}(n) = \frac{N!}{n!\,(N-n)!}\,p^n(1-p)^{N-n} \tag{2.13}$$

where p denotes the probability of detecting a photon in a single subinterval. This probability is equal to the average number of detected photons $\bar{n}$ in the observation interval divided by the number of subintervals N:

$$p = \frac{\bar{n}}{N} \tag{2.14}$$

Substituting this expression into Equation 2.13 yields:

$$\mathcal{P}(n) = \frac{N!}{n!\,(N-n)!}\left(\frac{\bar{n}}{N}\right)^{n}\left(1-\frac{\bar{n}}{N}\right)^{N-n} \tag{2.15}$$

In the limit $N \to \infty$, it can be shown [5] that the probability of detecting n photons in a coherent light beam reduces to:

$$\mathcal{P}(n) = \frac{\bar{n}^{\,n}}{n!}\,e^{-\bar{n}} \tag{2.16}$$

This result corresponds to a **Poisson distribution**, which is the characteristic photon-counting statistic of coherent light sources. A distinctive property of the Poisson distribution is that the mean photon number $\langle n\rangle$ is equal to its variance, i.e. $\langle n\rangle = \mathrm{Var}(n) = \bar{n}$.
Furthermore, it has been demonstrated that the coincidence counts of photon pairs generated via SPDC also follow a Poissonian distribution, since the SPDC process preserves the coherence of the incident pump laser [1, 10, 16]. Consequently, the variance of the total coincidence counts in Equation 2.12 can likewise be approximated by their mean value, $\mathrm{Var}(N_{\mathrm{tot,cc}}) \approx \langle N_{\mathrm{tot,cc}}\rangle$.

accidentals as well??

2.3.2. Thermal light

In contrast to coherent light sources, which exhibit Poissonian photon statistics, thermal light displays fundamentally different statistical properties. Thermal radiation arises from the random emission of photons in a hot body, where the optical field consists of a large number of independently oscillating modes. Each mode can occupy quantized energy levels depending on their angular frequency ω:

$$E_n = \left(n + \tfrac{1}{2}\right)\hbar\omega, \qquad n \geq 0, \tag{2.17}$$

where n denotes the photon occupation number.
Using the quantization of energy levels and Planck's law, the probability of finding n photons in a single mode is then governed by Boltzmann's law [5]:

$$\mathcal{P}_{\omega}(n) = \frac{\exp(-n\hbar\omega/k_BT)}{\sum_{m=0}^{\infty}\exp(-m\hbar\omega/k_BT)} \tag{2.18}$$

It can be shown that the mean photon number $\bar{n}$ can be expressed as [5]:

$$\bar{n} = \frac{1}{\exp(\hbar\omega/k_B T) - 1} \tag{2.19}$$

Substituting this expression into Equation 2.18, the probability distribution can be rewritten as follows:

$$\mathcal{P}_\omega(n) = \frac{1}{\bar{n}+1}\left(\frac{\bar{n}}{\bar{n}+1}\right)^n \tag{2.20}$$

This distribution is referred to as single-mode **Bose-Einstein distribution**.
In practice, thermal light sources generally populate a large number of independent modes. Consequently, the multi-mode expansion of the Bose-Einstein distribution must be considered. Assuming that m modes of the field are occupied and that the thermal light is fully unpolarized, the multi-mode Bose-Einstein (mmBE) distribution can be expressed as [14]:

$$\mathcal{P}_m(n) = \frac{(n+m-1)!}{(m-1)!\,n!}\,\frac{\bar{n}^n}{(1+\bar{n}/m)^m\,(\bar{n}+m)^n} \tag{2.21}$$

The combinatorial prefactor accounts for the number of ways in which n photons can be distributed among m modes, while the remaining factor describes the joint probability associated with the m occupied modes. As a consistency check, it is readily verified that for $m = 1$ the expression reduces to the single-mode Bose-Einstein distribution given in Equation 2.20.
The variance of the photon number in the mmBE distribution is given by:

$$\mathrm{Var}(n) = \bar{n}\left(1 + \frac{\bar{n}}{m}\right) \tag{2.22}$$

When compared to the Poissonian variance $\mathrm{Var}(n) = \bar{n}$, it is evident that the mmBE distribution always exhibits larger fluctuations. Hence, thermal light is intrinsically super-Poissonian. This property is commonly described in terms of photon bunching, meaning that photons tend to arrive in groups more frequently than would be expected for the random distribution characteristic of coherent (Poissonian) light.
From this perspective, coherent sources represent the most stable form of light in terms of intensity, while any source with time-dependent fluctuations, such as thermal radiation, necessarily shows enhanced photon-number fluctuations and thus super-Poissonian statistics.
In the limit $m \to \infty$, the variance of the mmBE distribution approaches the Poissonian result, as can be seen directly from Equation 2.22. This reflects the fact that in the presence of infinitely many modes, the photon statistics become indistinguishable from those of a coherent source.
It was shown that each photon from a SPDC process exhibits mmBE statistics, whether it is a signal or idler photon [10]. The mode number m and, consequently, the variance depend on the chosen setup and must be determined individually.

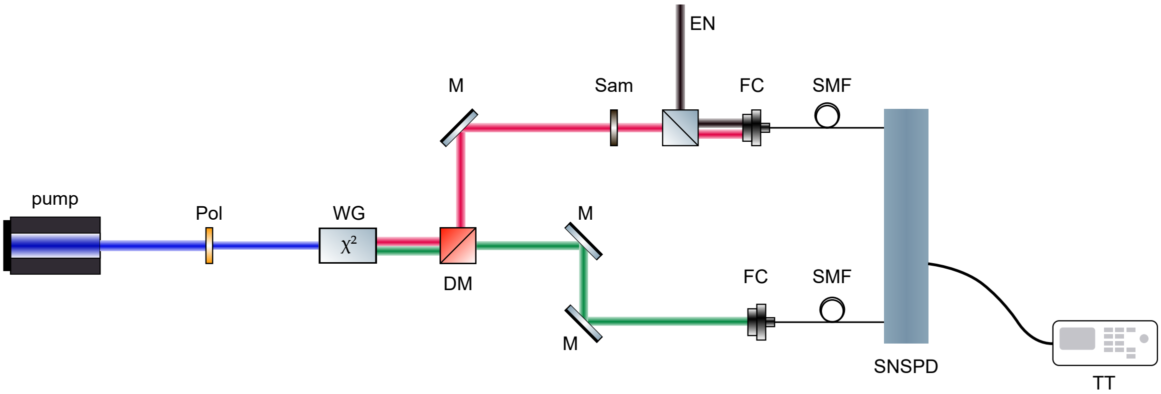

Figure 3.: Experimental setup: Explain components..

3. Experimental Setup

To establish a consistent model that predicts regions in which the coincidence approach is superior, the assumptions for the different unknown parameters (e.g., the variance of coincidence and accidental counts) must align with the results obtained in an experimental setup. Therefore, the following section explains the setup used to measure the statistics of the different parameters in more detail.
The setup consists of a BBO crystal that produces temporally correlated photon pairs using type-I/II? SPDC. The idler photon lies in the infrared at a wavelength of $\lambda_\mathrm{i} = 1400\mathrm{nm}$, while the signal photon is in the visible spectrum at a wavelength of $\lambda_\mathrm{s} = 650\mathrm{nm}$??. The crystal is pumped by a diode laser operating at $\lambda_\mathrm{p} = 405\mathrm{nm}$.
The idler photons are coupled to a IR single photon detector via multi-mode fiber, the signal photons to a single photon detector operating in the visible regime using a multi-mode fiber. Both detectors are connected to a time-tagging unit to obtain the coincidences between both arms. A sketch of the setup is shown in Figure 3. Has to aligned with Dupish's setup!!

4. Results

4.1. Coincidence-to-accidentals ratio

One issue that must be addressed when determining the statistics of the different parameters is that the Coincidence-to-Accidentals ratio (CAR) depends on the exposure time. Therefore, before measuring the statistical distributions, an exposure time must be found for which the CAR value remains constant. Thus, this value was measured for nine exposure times ranging from ten milliseconds to sixty seconds. The integration time was set to fifty times the exposure time for each measurement. Hence, ten histograms were saved for each exposure time and based on these histograms, the average CAR value and its standard deviation were calculated for each exposure time.

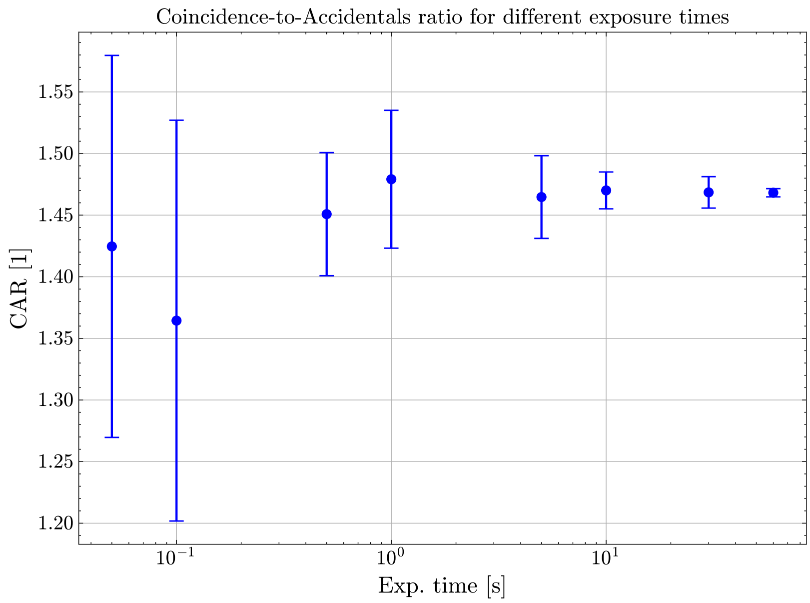

Figure 4.: Coincidence-to-Accidentals ration for different exposure times

The results are shown in Figure 4. As the exposure time increases, it can be seen that the fluctuation of the CAR value (i.e. its standard deviation) decreases. Furthermore, after an exposure time of one second, the CAR value remains approximately constant. Therefore, this range from one second onwards is preferred for statistical analysis. However, as this requires many consecutive and lengthy measurements, the aim is to use the shortest possible exposure time at which the CAR value remains constant. Therefore, one second will be used as the exposure time for upcoming measurements.

4.2. Heralding efficiencies

The heralding efficiency can be defined as the probability of detecting a photon in one arm given that a detection event has occurred in the other arm. For example, the heralding efficiency of the signal arm η_{sig}, conditioned on an idler detection, can be calculated using equations 2.2, 2.7 and 2.9:

$$\eta_{\text{sig}} = \frac{N_{\text{tot,cc}} - N_{\text{ac}}}{N_{\text{tot,idl}} - N_{\text{noise}}} = \frac{\eta_{\text{sig}}\eta_{\text{idl}}N_{\text{g}}}{\eta_{\text{idl}}N_{\text{g}}} \tag{4.1}$$

Analogously, the heralding efficiency of the idler arm η_{idl}, conditioned on the signal detection, is given by:

$$\eta_{\text{idl}} = \frac{N_{\text{tot,cc}} - N_{\text{ac}}}{N_{\text{tot,sig}} - N_{\text{noise}}} = \frac{\eta_{\text{sig}}\eta_{\text{idl}}N_{\text{g}}}{\eta_{\text{sig}}N_{\text{g}}} \tag{4.2}$$

It should be noted that the efficiency of the signal arm remains unchanged when a sample is placed in the idler arm. However, the efficiency of the idler arm itself decreases by a factor of T, the transmission.

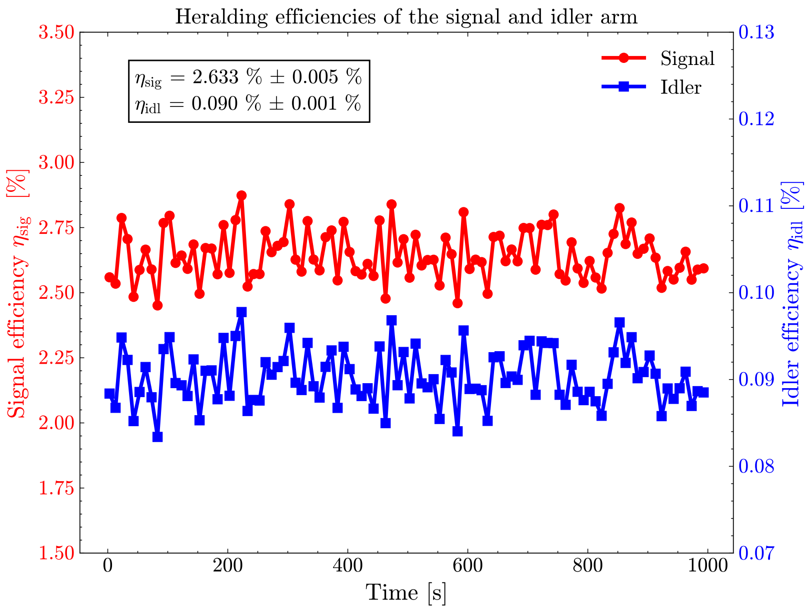

Figure 5.: Heralding efficiencies of the signal and idler arm

Both heralding efficiencies are crucial to assess the quality of the experimental setup, as they provide direct information about optical transmission losses and detector performance in each arm, and indirectly reflect the strength of photon-pair correlations. Efficiencies are also important when setting up the transmission model, as they are crucial for analytically calculating coincidence and accidental counts.

Representative values for the efficiencies were measured experimentally in the setup as they will be used in the analytical formulas. The exposure time was set to one second and the integration time to one thousand seconds. At each time step, the single counts and histogram were retrieved, and the efficiencies were calculated using equations 4.1 and 4.2. The measurement was repeated six times to obtain a statistical distribution of the efficiencies. The results are shown in Figure 5.

As can be seen, the efficiency of the idler arm is much smaller than that of the signal arm, at 0.09% and 2.63% respectively. The main reason for this difference may be the idler photons' low detection efficiency in the IR regime compared to the signal photons, which are in the visible range [Sources??]. The average value of the efficiencies and their standard deviation is displayed in the black box. As can be seen, the fluctuations of both values are quite small. These two experimentally obtained efficiencies are later used in the transmission model to compare the single and coincidence approach in a simulation.

4.3. Dark counts

exposure time: 100ms integration time: 5500s Repeats: 7 number of data points for each repeat: 55000 tbd..

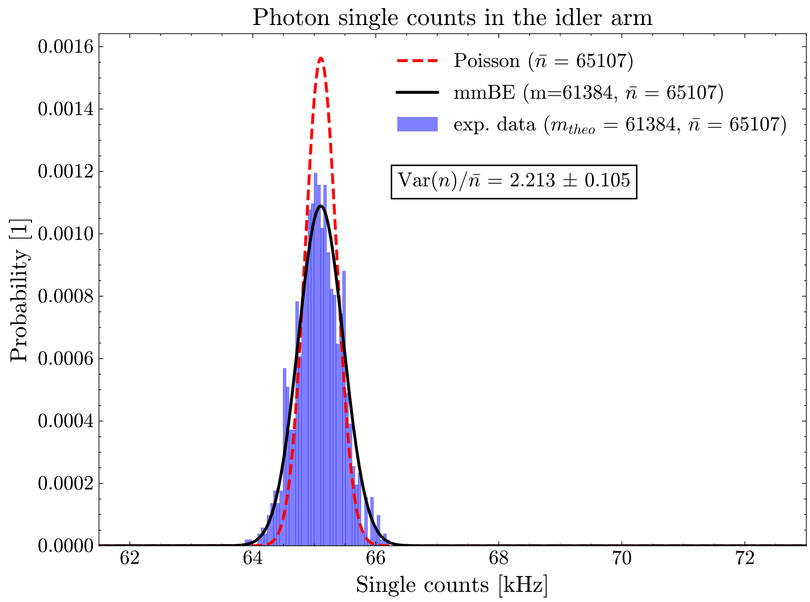

Figure 6.: Photon statistics in the idler arm

4.4. Single counts

To correctly model Equation 2.6 and the variance of the total photon counts (i.e.,$\mathrm{Var}\left(N_{\mathrm{tot}}^{\mathrm{ref}}\right)$ and $\mathrm{Var}(N_{\mathrm{tot}}^{\mathrm{sam}})$), the statistics of the idler arm were investigated experimentally.

For the measurement, the exposure time was set to one second and the integration time to one thousand seconds. Thus, each measurement yielded 1,000 data points for statistical analysis. The measurement was repeated five times to account for statistical fluctuations and determine an interval for the variance-to-mean ratio. The results of the measurements are shown in Figure 6.

The average photon number $\bar{n}$ is 65,107. Furthermore, the mode number m_{theo}, which was determined using the experimental variance value and Equation 2.22, is 61,384. Based on these two values, a mmBE and a Poisson distribution were modeled. As can be seen, the Poisson distribution significantly overestimates the peak of the experimental distribution. Additionally, the Poisson distribution decreases faster than the experimental distribution, so the edges of the distribution are not modeled correctly. On the other hand, the mmBE fit agrees much better with the experimental distribution because it properly estimates the peak and the edges of the experimental distribution fall within the theoretical fit.

The black box shows the variance-to-mean ratio for the five repeated measurements. The mean ratio value is 2.2, with a standard deviation of 0.1. Since this ratio is not equal to one, it confirms that the experimental distribution is not Poisson but has a higher variance. For the modeling of the variance of the single counts, this means that $\mathrm{Var}\left(N_{\mathrm{tot}}^{\mathrm{ref}}\right)$ and $\mathrm{Var}(N_{\mathrm{tot}}^{\mathrm{sam}})$ can be approximated by the mean photon number multiplied with a factor of 2.2.

As a consistency check, the statistics of the photons in the signal arm were also measured, as they should exhibit a mmBE distribution. The experimental parameters are kept the

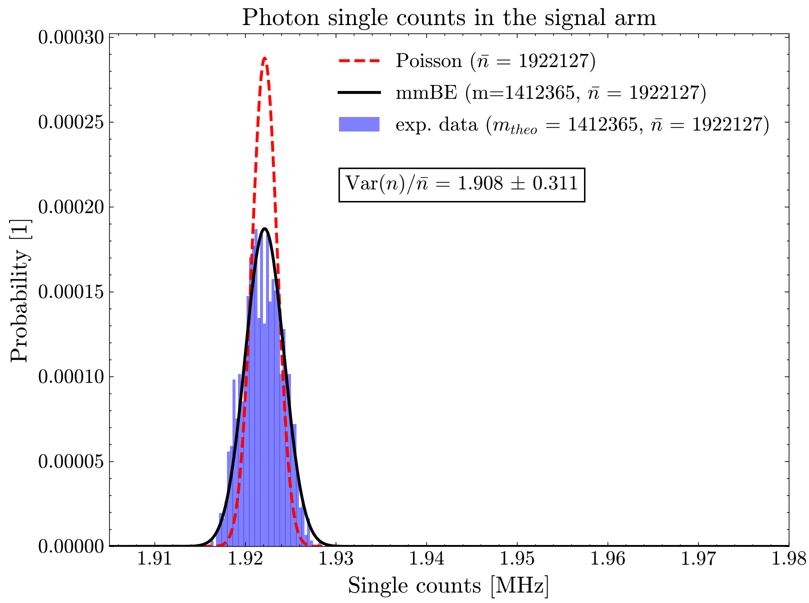

Figure 7.: Photon statistics in the signal arm

same as in the idler arm measurements.

The results can be seen in Figure 7. The approach for calculating the Poisson and mmBE distribution is the same as for the idler photons. Similar to the idler arm, the mmBE model more closely resembles the experimental distribution than the Poisson model because it overestimates the peak and underestimates the edges of the distribution. This is confirmed once more by calculating the variance-to-mean ratio, which yields an average of 1.9 and shows that the distribution is not Poissonian.
The count rate of the signal photons is roughly 30 times higher than the idler photons. The reason for this is the different sensitivity of the VIS and IR detector for the respective wavelength range. As a consequence, the mode number m_{theo} resulting from the experimental variance is also significantly larger.

Can I calculate m_{theo} in another way??

4.5. Coincidence counts

To determine the variance of the coincidence counts that are required to calculate the variance of the transmission in Equation 2.12, five measurements were performed. The experimental parameters were kept the same as in the previous section for the singles. Therefore, an exposure time of one second and an integration time of one thousand seconds was used. For every step in time, a histogram was saved by the time-tagging unit with a coincidence window of $\tau_{\text{cw}} = 9.36$ ns. A representative histogram can be seen in appendix tbd!!!.
The results of the measurements are shown in Figure 8. Similarly to the single counts, a

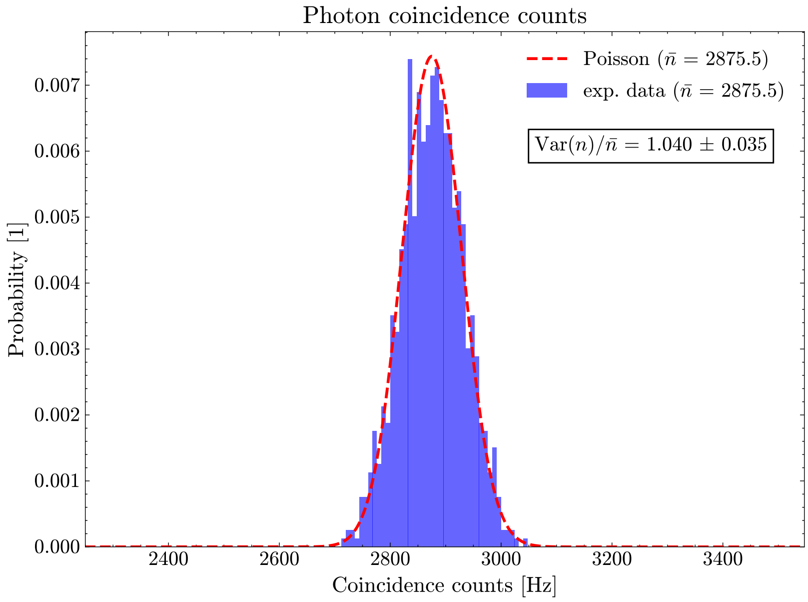

Figure 8.: Photon statistics of coincidence counts

Poisson distribution is modeled based on the average photon rate observed in the experiment. As can be seen, the experimental distribution is well approximated by the Poisson distribution. This is confirmed by considering the variance-to-mean ratio illustrated in the black box. An average value of 1.040 and a standard deviation of 0.035 are achieved for the five measurements. This coincides with the theoretical prediction in subsubsection 2.3.1 that coincidence counts can be approximated by a Poisson distribution where the variance equals the mean.
Consequently, the variance of the coincidence counts in the transmission model can be substituted by the average coincidence counts.

4.6. Accidental counts

Regarding accidental counts, two parameters have to be determined experimentally. Not only must the variance of the accidental counts be measured for Equation 2.12, but also Equation 2.8 for calculating them from single and coincidence counts.
For the variance measurement, the exposure time was set to one second and the integration time to sixty seconds. The histogram of the coincidences was used to retrieve the accidental counts. The bin width was set to 1400 and the number of bins was set to 110. The coincidence window was set to 2.8 ns, which means that two bins were selected as coincidence counts. To obtain just the accidental counts from each histogram, not only the two coincidence peaks, but also the two adjacent bins were neglected. This results in 6,300 accidental counts over the sixty time steps.
The statistical distribution is shown in Figure 9. Similar to previous results, a Poisson distribution was modeled based on average accidental counts. As can be seen, the Poissonian

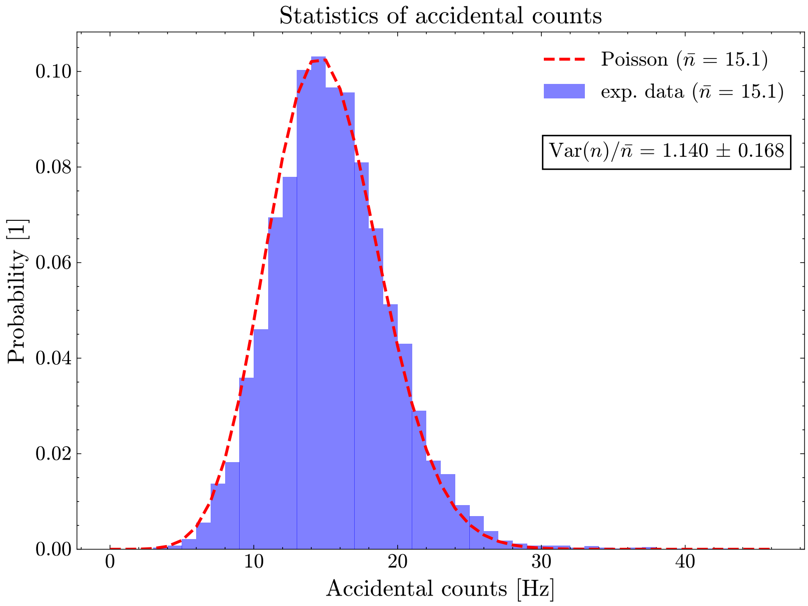

Figure 9.: Photon statistics of accidental counts

fit closely matches the experimental distribution.

To obtain a quantitative measure of the distribution in addition to a qualitative one, the variance-to-mean ratio was again calculated. For each time step, 105 values were obtained for the accidental counts, and the variance-to-mean ratio was determined. Then, the average and standard deviation of the ratio were calculated for the sixty steps. The result is shown in the black box of Figure 9.

Within the limits of the standard deviation, the ratio corresponds to one, which is the ratio of a Poisson distribution. Therefore, the accidental counts can be assumed to have a Poisson distribution, and the variance can be substituted by the average accidental count.

The second parameter that must be validated is whether the formula used to calculate the accidental counts is consistent with the counts measured experimentally. For this evaluation, histograms from the statistical analysis were used, as well as the single counts in each arm. I.e., the exposure time is one second and the integration time is sixty seconds. The bin width was set to 1400 and the coincidence window was 2.8 ns.

According to Equation 2.8, the accidental counts can be calculated at each time step using the single counts, coincidence counts and the coincidence window. This value is then compared with accidental counts measured experimentally. Again, in each time step, 105 values for the accidental counts were retrieved. In Figure 10, the theoretical values are compared with the experimental ones, where for the experimental counts the average and standard deviation is shown.

As can be seen, the theoretical values always fall within the standard deviation of the experimental counts. However, it is more important to consider whether the average value of the experimentally obtained counts can be well approximated by the formula, and thus, the

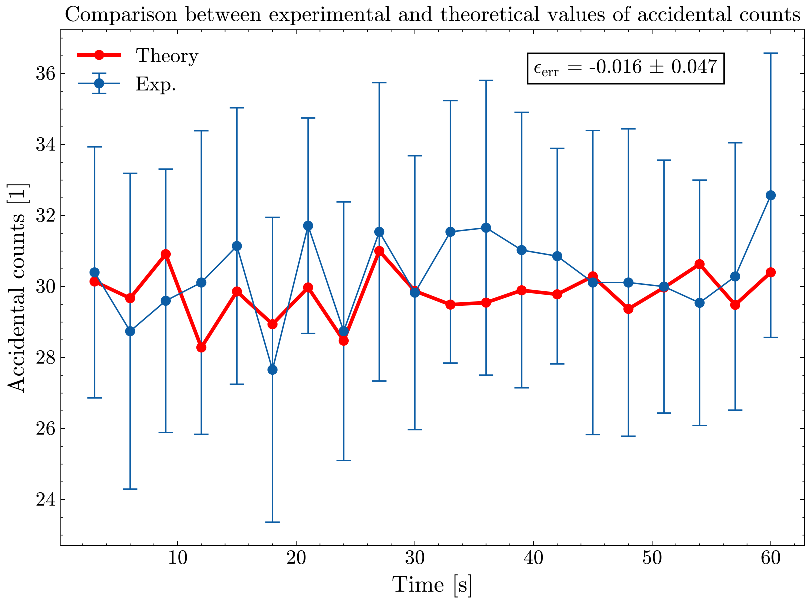

Figure 10.: Comparison between theoretically and experimentally obtained accidental counts

theoretical values. This is decisive as the theoretical value obtained from Equation 2.8 is the estimator of the accidental counts in the transmission model.
To determine the deviation between the theoretical value and the average of the experimental accidental counts, the relative error was calculated at each time step as follows:

$$\epsilon_{\text{err}} = \frac{R_{\text{acc}}^{\text{theo}} - R_{\text{acc}}^{\text{exp}}}{R_{\text{acc}}^{\text{exp}}} \tag{4.3}$$

In the black box in Figure 10, the mean value and standard deviation of the relative error for the sixty time steps is shown. As can be seen, the average relative error between the two values is 1.6 %, so the formula can be used as a good approximation given the experimental uncertainties.

As a consequence, all parameters that are important for the transmission model showed close agreement with the theoretical assumptions. As a next step, the approved model can be used to determine regions in which the coincidence approach offers an advantage compared to the one using single counts.

5. Simulation

tbd

6. Conclusion

Appendix A.

Supplemental Information

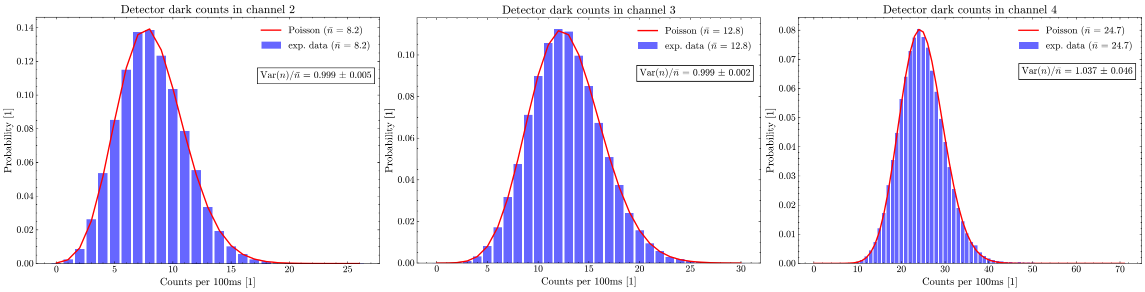

Figure A.1.: Dark counts of the SNSPD

List of Figures

List of Tables

Bibliography

[1] M. Avenhaus et al. “Photon Number Statistics of Multimode Parametric Down-Conversion”. In: *Physical Review Letters* 101.5 (Aug. 2008), p. 053601. ISSN: 0031-9007, 1079-7114. DOI: 10.1103/PhysRevLett.101.053601. (Visited on 08/28/2025).

[2] Robert W. Boyd. *Nonlinear Optics*. 3rd ed. Burlington, MA: Academic Press, 2008. ISBN: 978-0-12-369470-6.

[3] Hugo Defienne et al. “Advances in Quantum Imaging”. In: *Nature Photonics* 18.10 (Oct. 2024), pp. 1024–1036. ISSN: 1749-4885, 1749-4893. DOI: 10.1038/s41566-024-01516-w. arXiv: 2411.08415 [quant-ph]. (Visited on 08/28/2025).

[4] Marco Fiorentino et al. “Spontaneous Parametric Down-Conversion in Periodically Poled KTP Waveguides and Bulk Crystals”. In: *Optics Express* 15.12 (June 2007), pp. 7479–7488. ISSN: 1094-4087. DOI: 10.1364/OE.15.007479. (Visited on 09/03/2025).

[5] Mark Fox. *Quantum Optics: An Introduction*. Oxford Master Series in Physics 15. Oxford ; New York: Oxford University Press, 2006. ISBN: 978-0-19-856672-4 978-0-19-856673-1.

[6] Marta Gilaberte Basset et al. “Perspectives for Applications of Quantum Imaging”. In: *Laser & Photonics Reviews* 13.10 (2019), p. 1900097. ISSN: 1863-8899. DOI: 10.1002/lpor.201900097. (Visited on 09/03/2025).

[7] Majeed M. Hayat, Sergio N. Torres, and Leno M. Pedrotti. “Theory of Photon Coincidence Statistics in Photon-Correlated Beams”. In: *Optics Communications* 169.1 (Oct. 1999), pp. 275–287. ISSN: 0030-4018. DOI: 10.1016/S0030-4018(99)00384-3. (Visited on 09/05/2025).

[8] Genki Ishigane et al. “Label-Free Mid-Infrared Photothermal Live-Cell Imaging beyond Video Rate”. In: *Light: Science & Applications* 12.1 (July 2023), p. 174. ISSN: 2047-7538. DOI: 10.1038/s41377-023-01214-2. (Visited on 09/10/2025).

[9] Ryo Kato et al. “Label-Free Visualization of Photosynthetic Microbial Biofilms Using Mid-Infrared Photothermal and Autofluorescence Imaging”. In: *Analyst* 148.24 (Dec. 2023), pp. 6241–6247. ISSN: 1364-5528. DOI: 10.1039/D3AN01453C. (Visited on 09/10/2025).

[10] Jin-Woo Kim et al. “Photon-Counting Statistics-Based Support Vector Machine with Multi-Mode Photon Illumination for Quantum Imaging”. In: *Scientific Reports* 12.1 (Oct. 2022), p. 16594. ISSN: 2045-2322. DOI: 10.1038/s41598-022-20501-3. (Visited on 09/09/2025).

[11] H.H. Ku. “Notes on the Use of Propagation of Error Formulas”. In: *Journal of Research of the National Bureau of Standards, Section C: Engineering and Instrumentation* 70C.4 (Oct. 1966), p. 263. ISSN: 0022-4316. DOI: 10.6028/jres.070C.025. (Visited on 09/05/2025).

[12] Paul G. Kwiat et al. “Ultrabright Source of Polarization-Entangled Photons”. In: *Physical Review A* 60.2 (Aug. 1999), R773–R776. DOI: 10.1103/PhysRevA.60.R773. (Visited on 09/03/2025).

[13] Gabriela Barreto Lemos et al. “Quantum Imaging with Undetected Photons”. In: *Nature* 512.7515 (Aug. 2014), pp. 409–412. ISSN: 1476-4687. DOI: 10.1038/nature13586. (Visited on 09/10/2025).

[14] Leonard Mandel and Emil Wolf. *Optical Coherence and Quantum Optics*. Cambridge: Cambridge University Press, 1995. ISBN: 978-0-521-41711-2. DOI: 10.1017/CBO9781139644105. (Visited on 09/09/2025).

[15] Paul-Antoine Moreau et al. “Imaging with Quantum States of Light”. In: *Nature Reviews Physics* 1.6 (May 2019), pp. 367–380. ISSN: 2522-5820. DOI: 10.1038/s42254-019-0056-0. (Visited on 08/28/2025).

[16] James Schneeloch et al. “Introduction to the Absolute Brightness and Number Statistics in Spontaneous Parametric Down-Conversion”. In: *Journal of Optics* 21.4 (Feb. 2019), p. 043501. ISSN: 2040-8986. DOI: 10.1088/2040-8986/ab05a8. (Visited on 09/09/2025).

[17] S. Tanzilli et al. *Highly Efficient Photon-Pair Source Using a Periodically Poled Lithium Niobate Waveguide*. Dec. 2000. DOI: 10.48550/arXiv.quant-ph/0012053. arXiv: quant-ph/0012053. (Visited on 09/03/2025).